Supplemental Information

Supplemental Data

Table S1, Related to Figure 1. Acetyl occupancy quantitation data for each tissue. Tab 2 contains all acetyl sites that have fold changes with associated p values of less than or equal to 0.05.

Table S2, Related to Figure 1. Protein quantitation data. Tab 2 contains proteins that have fold changes with associated p values of less than or equal to 0.05.

Figure S1. Acetyl site and protein data analysis, Related to Figure 1. (A) Bimodal distributions of acetyl sites quantified separate mitochondrial (white) and non-mitochondrial (blue) acetyl sites. Mice lacking SIRT3 exhibit marked hyperacetylation of predominantly mitochondrial acetyl sites, indicating the major role of SIRT3 in the five tissues analyzed is mitochondrial. (B) Distribution of fold change between *Sirt3*$^{-/-}$ and WT indicates little change in overall distribution of protein-fold changes in each tissue.

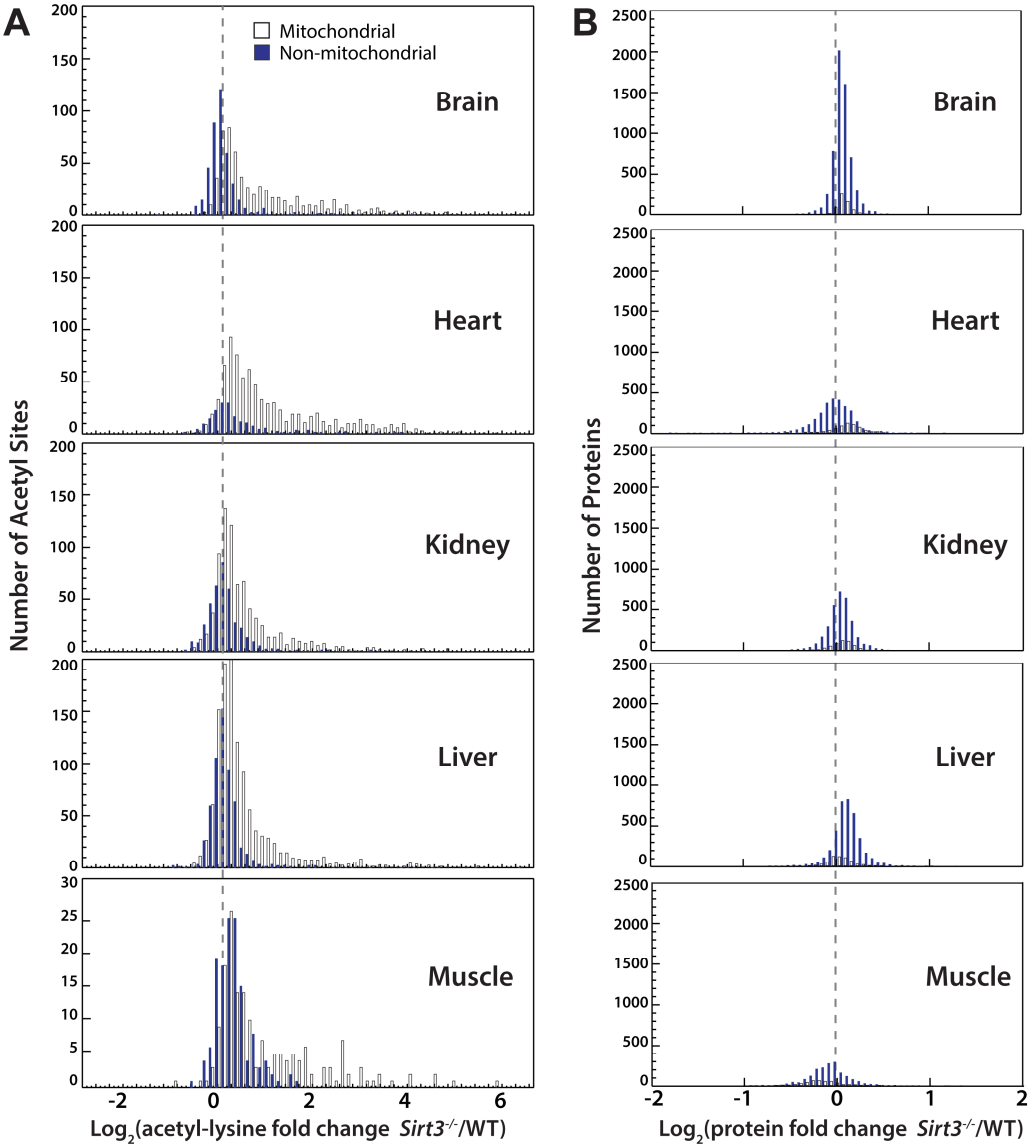

Figure S2, related to Figure 2. Western blot of whole tissue lysate from WT animals used in proteome analysis confirms targeted proteomics results of tissue variation in SIRT3 expression. SIRT3 protein expression levels were assessed using an anti-SIRT3 antibody and normalized to mitochondrial protein level with an anti-VDAC1 antibody. Representative blot, each lane per tissue corresponds to one WT animal, n = 3.

Figure S3, Related to Figure 3. Tissue similarities determined for each cluster generated by Gaussian mixture model algorithm. Each cluster and associated dendrogram is depicted with Euclidean distance measurements. Clusters display distinct profiles with extra-hepatic and hepatic tissues grouping together in each cluster.

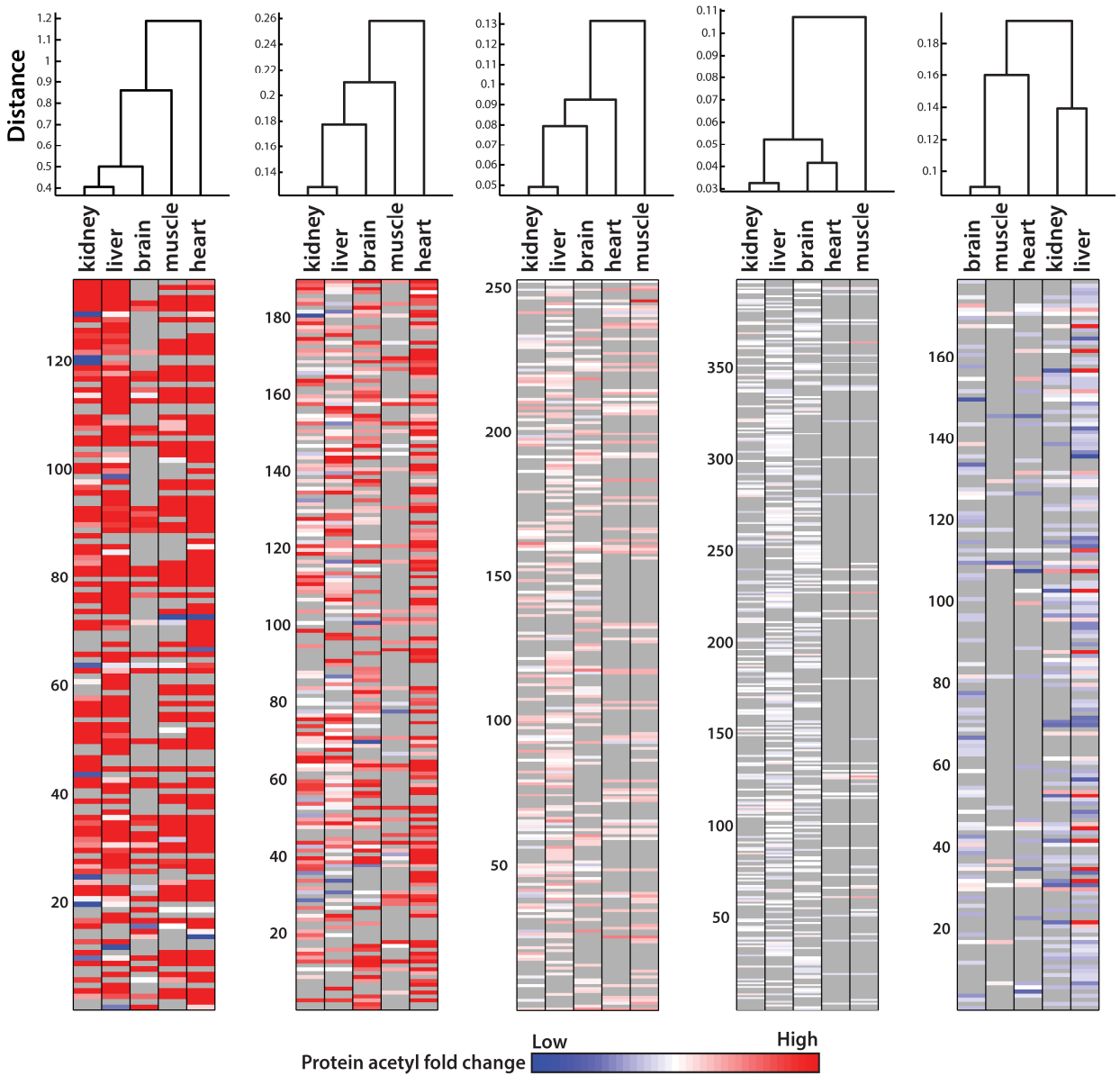

Figure S4, Related to Figure 4. (A) Cluster analysis of acetyl sites identified in all tissues identifies highly probably SIRT3 targets. **(B)** Direct comparison of QSSA results and DAVID KEGG pathway enrichment results.

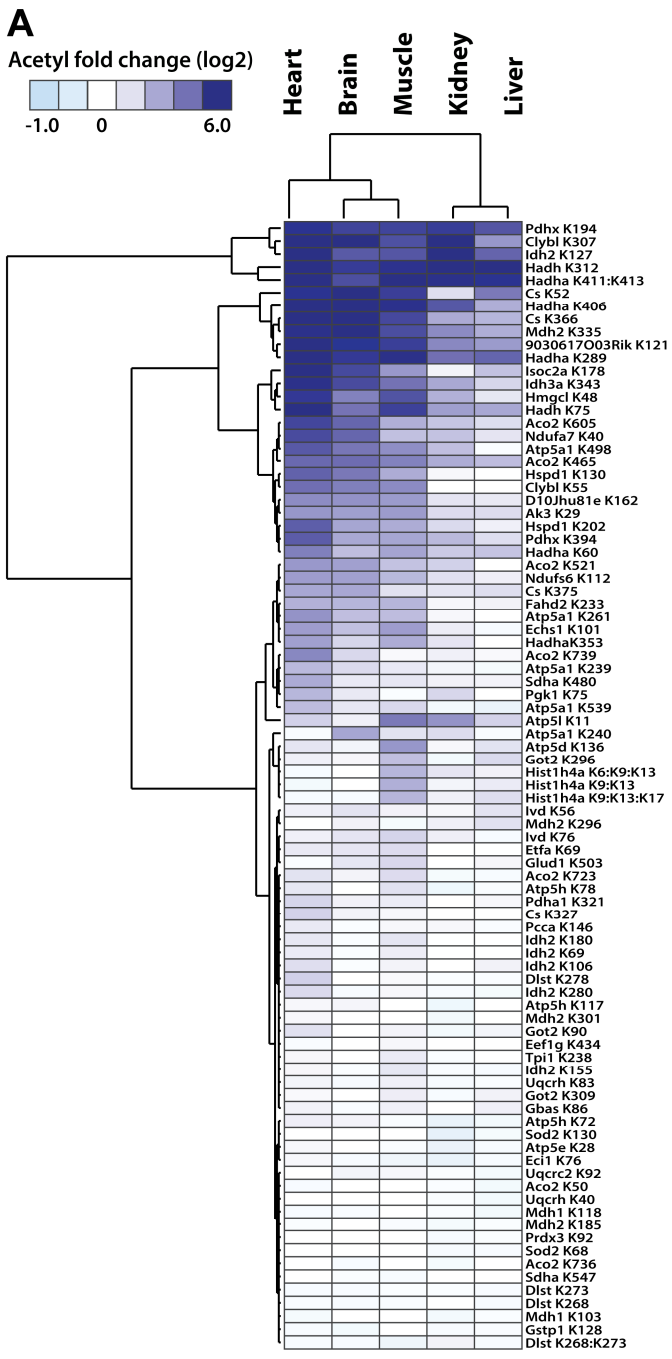

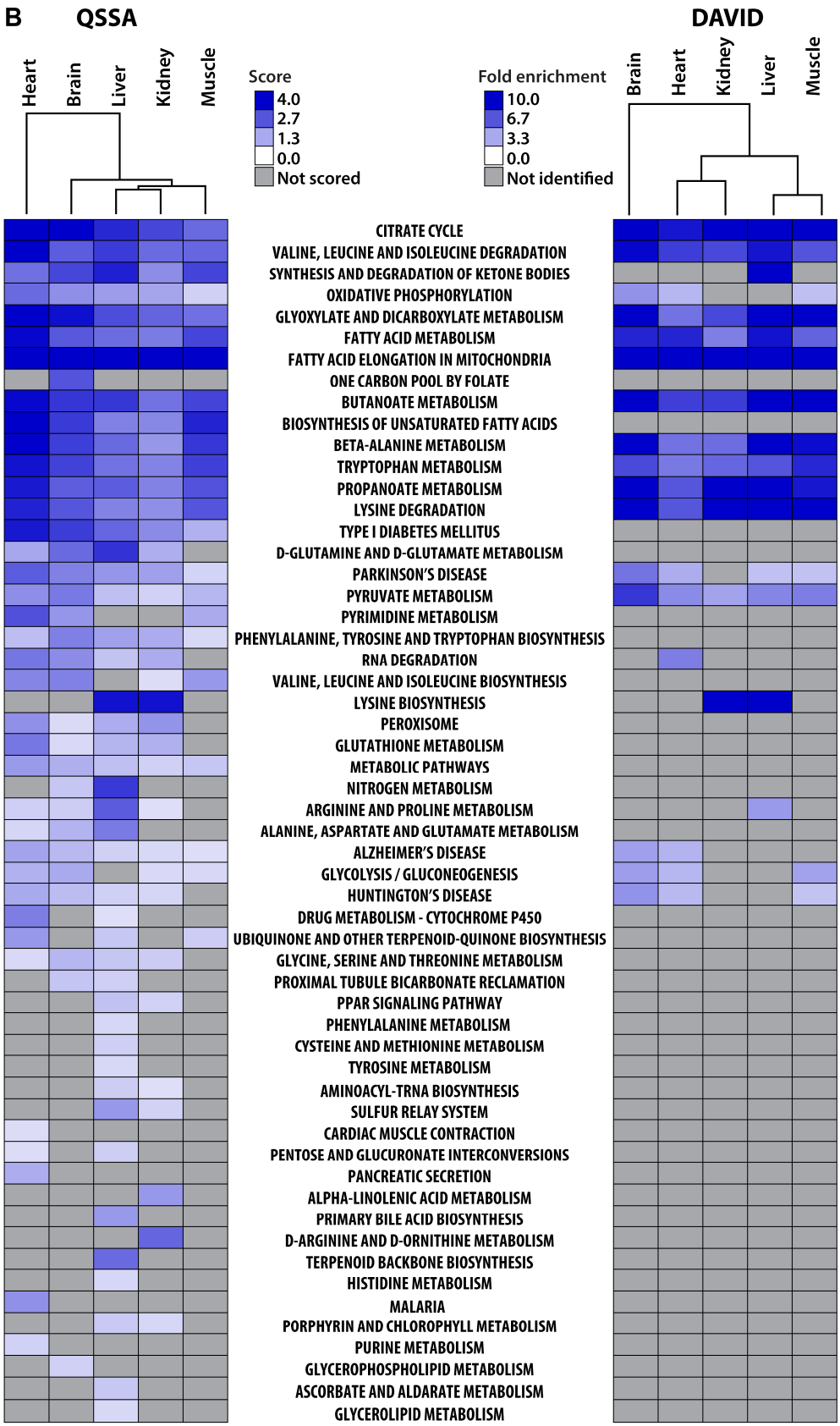
B
QSSA
DAVID
Heart
Brain
Liver
Kidney
Muscle
Score
4.0
2.7
1.3
0.0
Not scored
Fold enrichment
10.0
6.7
3.3
0.0
Not identified
CITRATE CYCLE
VALINE, LEUCINE AND ISOLEUCINE DEGRADATION
SYNTHESIS AND DEGRADATION OF KETONE BODIES
OXIDATIVE PHOSPHORYLATION
GLYOXYLATE AND DICARBOXYLATE METABOLISM
FATTY ACID METABOLISM
FATTY ACID ELONGATION IN MITOCHONDRIA
ONE CARBON POOL BY FOLATE
BUTANOATE METABOLISM
BIOSYNTHESIS OF UNSATURATED FATTY ACIDS
BETA-ALANINE METABOLISM
TRYPTOPHAN METABOLISM
PROPANOATE METABOLISM
LYSINE DEGRADATION
TYPE I DIABETES MELLITUS
D-GLUTAMINE AND D-GLUTAMATE METABOLISM
PARKINSON'S DISEASE
PYRUVATE METABOLISM
PYRIMIDINE METABOLISM
PHENYLALANINE, TYROSINE AND TRYPTOPHAN BIOSYNTHESIS
RNA DEGRADATION
VALINE, LEUCINE AND ISOLEUCINE BIOSYNTHESIS
LYSINE BIOSYNTHESIS
PEROXISOME
GLUTATHIONE METABOLISM
METABOLIC PATHWAYS
NITROGEN METABOLISM
ARGININE AND PROLINE METABOLISM
ALANINE, ASPARTATE AND GLUTAMATE METABOLISM
ALZHEIMER'S DISEASE
GLYCOLYSIS / GLUCONEOGENESIS
HUNTINGTON'S DISEASE
DRUG METABOLISM - CYTOCHROME P450
UBIQUINONE AND OTHER TERPENOID-QUINONE BIOSYNTHESIS
GLYCINE, SERINE AND THREONINE METABOLISM
PROXIMAL TUBULE BICARBONATE RECLAMATION
PPAR SIGNALING PATHWAY
PHENYLALANINE METABOLISM
CYSTEINE AND METHIONINE METABOLISM
TYROSINE METABOLISM
AMINOACYL-TRNA BIOSYNTHESIS
SULFUR RELAY SYSTEM
CARDIAC MUSCLE CONTRACTION
PENTOSE AND GLUCURONATE INTERCONVERSIONS
PANCREATIC SECRETION
ALPHA-LINOLENIC ACID METABOLISM
PRIMARY BILE ACID BIOSYNTHESIS
D-ARGININE AND D-ORNITHINE METABOLISM
TERPENOID BACKBONE BIOSYNTHESIS
HISTIDINE METABOLISM
MALARIA
PORPHYRIN AND CHLOROPHYLL METABOLISM
PURINE METABOLISM
GLYCEROPHOSPHOLIPID METABOLISM
ASCORBATE AND ALDARATE METABOLISM
GLYCEROLIPID METABOLISM

Figure S5, Related to Figure 5. Rates of acetyl-CoA production, normalized citrate formation in brain cortex homogenates and normalized ketogenesis rate in liver homogenates from WT and *Sirt3*$^{-/-}$ animals. (A) Rates of acetyl-CoA production normalized to total protein concentration. Left, WT rates: Middle, *Sirt3*$^{-/-}$ rates: Right, Average rates (n = 3) for WT and *Sirt3*$^{-/-}$, One outlier (modified Thompson tau technique) was removed from *Sirt3*$^{-/-}$ data in average rate plot. Error bars show standard deviation of mean. (B) Citrate concentration was measured by mass spectrometry-metabolomics at 1 minute and 10 minutes. After 10 minutes, when most of the acetyl-CoA is consumed, oxaloacetate-dependent citrate formation is dramatically higher in three WT animals when compared to *Sirt3*$^{-/-}$ animals. (C) Liver homogenate-catalyzed CoA formation from acetyl-CoA was measured by LC-MS at indicated time points to determine the rate of ketogenesis in the liver. Results are normalized to total protein concentration. Left: WT rates; Right: *Sirt3*$^{-/-}$ rates. Bottom Left: Average acetyl-CoA-dependent CoA production; Bottom right: average rates. Error bars represent standard deviation of mean (n=4).

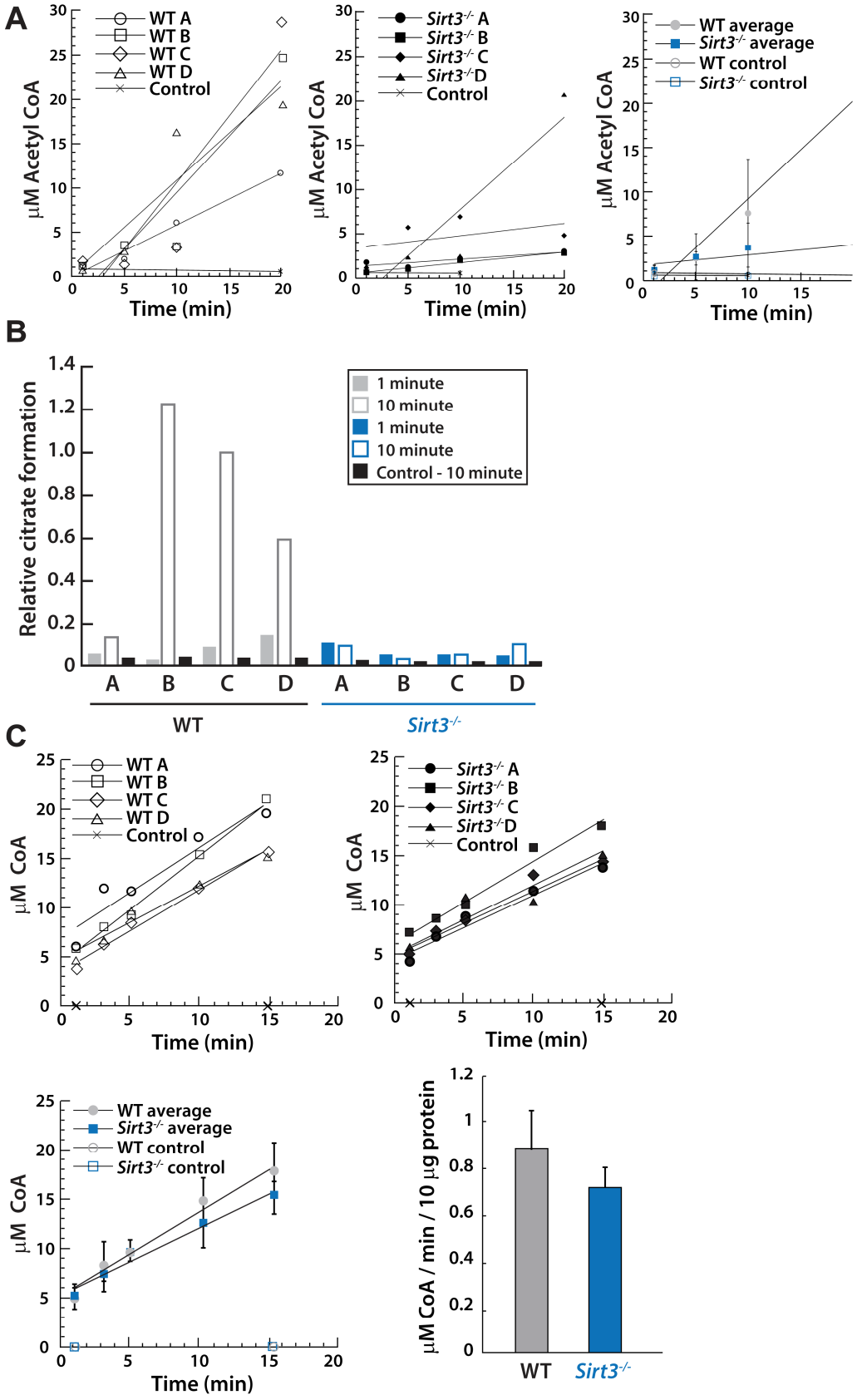
A
WT A
WT B
WT C
WT D
Control
Sirt3-/- A
Sirt3-/- B
Sirt3-/- C
Sirt3-/-D
Control
WT average
Sirt3-/- average
WT control
Sirt3-/- control
µM Acetyl CoA
Time (min)
B
Relative citrate formation
1 minute
10 minute
1 minute
10 minute
Control - 10 minute
A B C D A B C D
WT
Sirt3-/-
C
µM CoA
Time (min)

Figure S6, related to Figure 5. Recombinant OXCT analysis. (A) Successful expression and purification of acetylated OXCT confirmed by anti-acetyl lysine western blot on fractions eluted from nickel column. (B) Top: Anti-acetyl lysine western blot analysis of wild type OXCT and acetylated OXCT indicates OXCT is acetylated. Minimal deacetylation of acetylated OXCT in native conformation is observed with 10 hour SIRT3 treatment in the presence of NAD^+. Bottom: Anti-His tag loading control. (C) LC-MS measurement of Sirtuin product, *O*-acetyl-ADP-ribose, indicates SIRT3 deacetylates acetylated OXCT after minimal proteolytic digestion with trypsin. OXCT and TFAM (8 μM) were treated with trypsin (1:100) for 4 hours and peptides were separated from trypsin with a 10kDa spin filter. Peptides were incubated with 2 μM SIRT3 and 100 μM NAD at 37°C for the indicated times. Acetylated TFAM is used as a positive control. (D, E) Michaelis-Menten traces of wild type OXCT, acetylated OXCT and acetylated OXCT treated with SIRT3. Error bars represent standard deviation of mean. (F) Table summarizing kinetic parameters of activity assays.

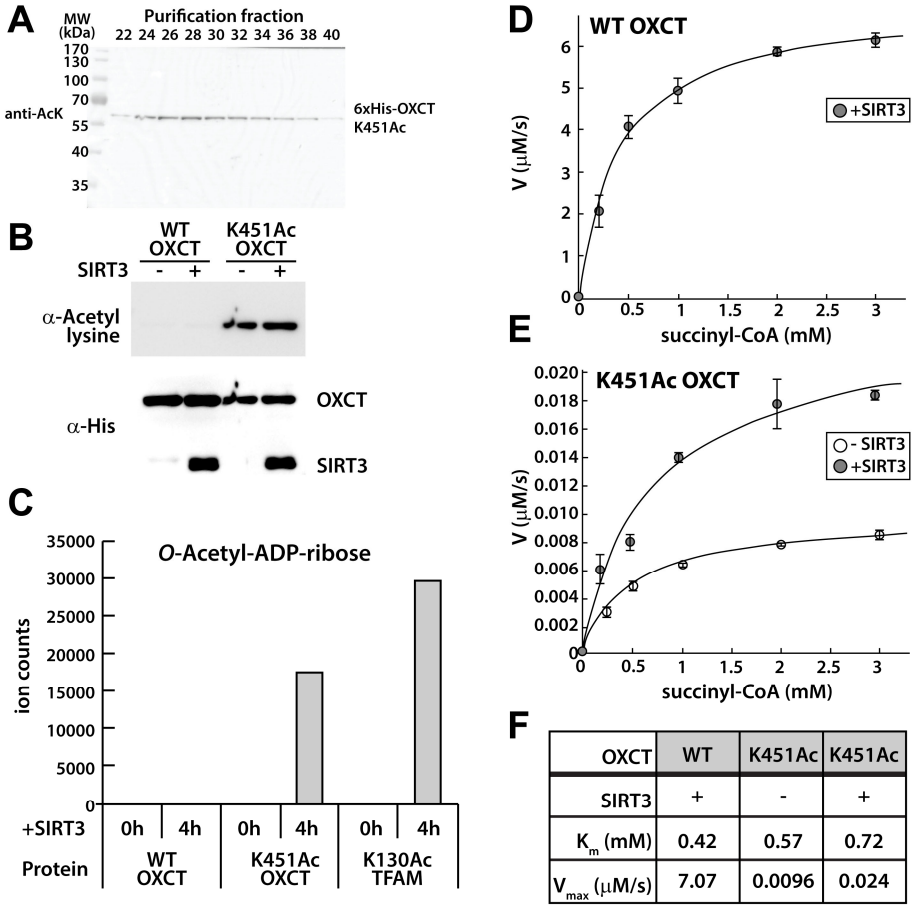

F

OXCT	WT	K451Ac	K451Ac
SIRT3	+	-	+
K_m (mM)	0.42	0.57	0.72
V_{max} (μM/s)	7.07	0.0096	0.024

Supplemental Experimental Procedures

Animals and Fasting Treatment

To establish the *Sirt3*$^{-/-}$ mouse colony, male and female *Sirt3*$^{+/-}$ mice were purchased from the Mutant Mouse Resource Centers (MMRRC) at the University of North Carolina-Chapel Hill. Exon one of one allele of the *Sirt3* gene was functionally inactivated using a retroviral promoter trap in embryonic stem cells. *Sirt3*$^{+/-}$ mice were backcrossed for at least four generations onto the C57BL/6J background. Age matched 5 month old *Sirt3*$^{-/-}$ were housed together while colony control WT mice were housed in separate cages. After a 24 hour fast (9AM to 9AM), mice were euthanized by decapitation and tissues were harvested from the mice and immediately frozen in liquid nitrogen. All animal studies were conducted at the AAALAC-approved Animal Facility in the Genetics and Biotechnology Center of the University of Wisconsin-Madison. Experiments were performed in accordance with protocols approved by the University of Wisconsin-Madison Institutional Animal Care and Use Committee and the Institutional Animal Care (Madison, WI).

Sample preparation and mass spectrometry

Sample Preparation

Tissue samples were resuspended in lysis buffer composed of 40 mM tris (pH 8.0), 15 mM NaCl, 1 mM $CaCl_2$, 300 mM sucrose, 0.1 mM EDTA, 10 mM sodium butyrate, 10 mM nicotinamide, and protease (Roche) and phosphatase inhibitor tablets (Roche). Tissues were lysed by glass bead milling (Retsch). Briefly, each tissue was resuspended in approximately 2 mL of lysis buffer and combined with 2 mL of acid washed glass beads in a stainless steel container and shaken 8 times at 30 hz for 4 min

with a 1 min rest in between. Lysates were centrifuged at 700xg and the pellet was discarded. Lysate protein concentration was measured by BCA (Thermo Pierce, Rockford, IL). Urea was added to each tissue sample to a final concentration of 8 M. 1 mg of protein from each sample was reduced by the addition of 5 mM dithiothreitol (DTT) and incubated for 45 min at room temperature. Free thiols were alkylated by the addition of 15 mM iodoacetamide (IAA) in the dark for 30 min. The alkylation reaction was quenched with 5 mM DTT. Urea concentration was diluted to 1.5 M with 50 mM Tris (pH 8.0). Proteins were digested with trypsin (Promega, Madison, WI) at a 1:50 enzyme to protein ratio and incubated at ambient temperature overnight. An additional aliquot of trypsin at a 1:50 ratio was added in the morning and incubated at ambient temperature for 1 h. The digestion was quenched by addition of TFA and desalted over a tC18 Sep-Pak (Waters, Milford, MA). TMT labeling was carried out according to the manufacturer's instructions (Thermo Pierce). Following tagging, proteins were mixed in a 1:1:1:1:1:1 ratio according to BCA results. For the targeted experiment, peptides from each WT1 mouse tissue were TMT labeled and mixed in a 1:1:1:1:1 ratio according to BCA results.

Fractionation

Strong cation exchange (SCX) fractionation was carried out using a polysulfoethylaspartamide column (9.4 x 200 mM, PolyLC) on a Surveyor LC quarternary pump at a flow rate of 3.0 mL/min. Tagged samples were resuspended in buffer A and separated over the following gradient: 0-2 min, 100% buffer A, 2-5 min, 0-15% buffer B, 5-35 min, 15-100% buffer B. Buffer B was then held at 100% for 10 min. The column was washed with buffer C and water and re-equilibrated after each use.

The following buffer compositions were used: buffer A: 5 mM KH_2PO_4, 30% acetonitrile (pH 2.6), buffer B: 5 mM KH_2PO_4, 30% acetonitrile, 350 mM KCl (pH 2.6), buffer C: 50 mM KH_2PO_4, 500 mM KCl (pH 7.5). 10-12 fractions were collected per tissue, frozen, lyophilized and desalted by Sep-Pak. 5% of total protein from each fraction was used for protein abundance measurements. The remaining protein was subject to immunopurification to isolate acetylated peptides.

Enrichment

The remaining protein was pooled into 6 fractions for acetyl lysine enrichment. Fractions were resuspended in 1 mL of 50 mM HEPES (pH 7.5) and 100 mM NaCl. 50 µL of pan-acetyl lysine antibody-agarose conjugate was added to each sample. Samples were rotated overnight at 4°C, washed eight times with 500 µL of 50 mM HEPES and 100 mM NaCl, and acetylated peptides were eluted with 0.1% TFA. The recovered peptides were desalted by Sep-Pak.

LC-MS/MS

Online reversed phase chromatography was performed using a NanoAcquity UPLC system (Waters, Milford, MA). Reversed phase columns were packed in-house using 75 µm (inner diameter) 360 µm (outer diameter) bare fused silica capillaries with laser pulled electrospray tips. Columns were packed to a length of 35 cm with 1.7 µm diameter, 130 angstrom pore size Bridged Ethylene Hybrid C18 particles (Waters). Columns were heated to 60 ° C for all runs. Mobile phase buffer A was composed of water, 0.2% formic acid, and 5% DMSO. Mobile phase B was composed of acetonitrile, 0.2% formic acid, and 5% DMSO. Samples were loaded onto the column for 12 min at

0.35 µl/min. Mobile phase B increases to 4% in the first 0.1 min then to 12% B at 32 min, 22% B at 60 min, and 30% B at 70 min, followed by a 5 min wash at 70% B and a 20 min re-equilibration at 0% B. Eluting peptide cations were converted to gas-phase ions by electrospray ionization and analyzed on a Thermo Orbitrap Fusion (Q-OT-qIT, Thermo). Survey scans of peptide precursors from 350 to 1600 *m*/*z* were performed at 60K resolution (at 200 *m*/*z*) with a 5×10^5 ion count target. Tandem MS was performed by isolation at either 0.7 or 1 Th with the quadrupole and HCD fragmentation with a normalized collision energy of 37. Analysis was performed in the Orbitrap at a resolution of either 30K or 60K. The MS^2 ion count target was set to 1×10^5. Precursors with a charge state of 2–8 were selected for MS^2 analysis. The dynamic exclusion duration was set to 30 s with a 10 ppm tolerance around the selected precursor and its isotopes. Monoisotopic precursor selection was turned on. The instrument was run in top speed mode with either 3 s or 5 s cycles. For targeted analysis, the peptide ASGIPASK (+2, *m/z* 594.864) was isolated over a 1 Th window. For targeted analysis, an inclusion mass list was compiled, with the appearance of peptide ASGIPASK (+2, *m/z* 594.864) triggering an MS^2 event. The precursor of interest was isolated in the quadrupole over a 1 Th window and analyzed in the Orbitrap at a resolution of 60K.

Database searching

All MS/MS data was analyzed using the Coon OMSSA Proteomics Software Suite (COMPASS)(Wenger et al., 2011). Spectra were searched using the Open Mass Spectrometry Search Algorithm (OMSSA)(Geer et al., 2004) against a concatenated taget-decoy database consisting of mouse protein sequences downloaded from UniProt. Tryptic peptides were created *in silico* allowing up to three missed cleavages.

Mass tolerance was set to 20 ppm for precursors and 0.01 Th for fragment ions. Oxidation of methionine (+15.994915) and TMT 6-plex on tyrosine (+229.162932) were searched as variable modifications. Carbamidomethylation (+57.021464) of cysteines, TMT 6-plex on lysine (+229.162932) and N-terminus (+229.162932) were searched as fixed modifications. For acetyl enriched peptides, a variable acetyl modification (-187.1523 Da) was also searched. This mass shift corresponds to the difference between an acetyl group and a TMT tag. Results were filtered to 1% FDR at the unique peptide level. TMT labeled peptides were quantified using TagQuant according to previously published procedures. Peptides were combined into protein groups and filtered to 1% FDR. Proteins were quantified by summing the intensity of the reporter ion tags of each channel for each protein. Acetylated peptides and peptides belonging to multiple protein groups were omitted from quantitation.

Acetylation normalization

Acetylation events were localized according to probabilistic methods. For all peptide spectral matches (PSMs) containing an acetylation modification, theoretical fragment spectra were generated for each possible isoform. Theoretical spectra were then compared to the experimental spectra at a 10 ppm threshold. The number of matching peaks between spectra were documented and a p-value was calculated using a cumulative binomial distribution. An AScore, or the difference between p-values, was calculated for each possible isoform, with acetylation sites considered localized if all AScores for a particular isoform were larger than the minimum value (AScore = 13, p-value < 0.05) for every comparison. All peptides with identical acetylation sites were grouped together, and their reporter ion intensities were summed.

Protein normalization

All quantitative measurements were Log2 transformed and mean normalized. Acetyl expression levels are normalized to their corresponding unmodified protein by subtracting the quantitative value of the unmodified protein from the reporter ion intensity of the acetylation site. Fold changes were determined by averaging the protein normalized values for each condition and calculating a difference of averages.

Clustering

To cluster the protein data set (~1100 proteins in 5 tissues) we used a Gaussian mixture model clustering approach with consensus clustering. Due to the large number of missing values (85% of proteins having missing values in two or more tissues), prior to applying the clustering method we interpolate the missing value with the mean of the non-missing values of the same protein.

Consensus clustering of multi-tissue protein data

To cluster the data we use Gaussian Mixture Model (GMM) (Hastie et al., 2009) with consensus clustering. Like most clustering methods, GMM finds a local minima and therefore different random initializations can produce slightly different clusters. To produce more robust clusters, we used GMM clustering within a consensus clustering framework (Nguyen, 2007).

The GMM clustering algorithm clusters a dataset of N proteins with D measurements into K clusters. We selected $K = 5$ for our experiments. Because our final set of clusters are the result of consensus clustering (defined below), our final set of clusters in not sensitive to the initial number of clusters. The assumption in GMM is that each cluster

has a multivariate Gaussian distribution (D dimensions), each dimension corresponding to a tissue. When estimating the parameters of the Gaussian distribution, we assume that the covariance matrix is diagonal (we only estimate the diagonal elements of the covariance matrix).

To produce the consensus clusters, we clustered the data set using GMM 100 times, and used hierarchical agglomerative clustering (HAC) on a co-clustered similarity matrix, S. Let $C_{i,j}$ be the number of times that proteins i and j were clustered together. We define each entry of S as $S_{i,j} = \frac{C_{i,j}}{100}$ and use this similarity matrix to perform HAC. We used a threshold of 0.6 to define the clusters such that on average, the proteins in each of the consensus clusters were clustered together 60% of the time or more.

Handling missing values

Before applying the clustering method, we interpolated the missing measurements of a protein using the average of non-missing values of the same protein. Let $\boldsymbol{u}_i$ be the set of tissues for which the i^{th} protein's values are not missing. Let denote p_j^i the measured value of the i^{th} protein in the j^{th} tissue. We interpolate the missing values of i as:

for $j \notin \boldsymbol{u}_i$: $p_j^i = \frac{\sum_{j' \in \boldsymbol{u}_i} p_{j'}^i}{|\boldsymbol{u}_i|}$

We experimented with Expectation Maximization-based missing value interpolation strategies, however, we found that this simple interpolation scheme gave the best results in terms of the size of the different clusters and the biological processes associated with each cluster.

Tissue clustering for each K cluster

After applying our consensus clustering approach we obtained 5 clusters. We next

reordered the columns/tissues of each cluster using hierarchical clustering using Euclidean metric for distance. Because of missing values, the same tissue may not have the same number of proteins. To handle this we defined the Euclidean distance between any pair of tissues using only those proteins that were measured in both tissues. Let v_j be the index of the proteins that are not missing the j^{th} tissue:

$$v_j = \{i : j^{th}\ tissue\ is\ not\ missing\ in\ p^i\}$$

We calculate the pairwise Euclidean distance of columns (tissues) j and j' and normalize it by the number of proteins with observed value in both j and j':

$$d_{j,j'} = \frac{\sqrt{\sum_{k \in v_j \cap v_{j'}} \left(p_j^k - p_{j'}^k\right)^2}}{\left|v_j \cap v_{j'}\right|}$$

This distance is used as input to hierarchical clustering with average linkage, and tissues are arranged based on the order in which they are merged by the clustering as shown in the dendrograms.

QSSA biological pathway analysis

To construct the gene set background used for the analysis we removed the UniProt accession identifications not identified in our LC-MS dataset from the KEGG pathway map. Then, for each gene remaining in the KEGG pathway map we obtained the protein sequence from the UniProt database, and summed the number of lysines per pathway. For each tissue we summed the number of acetyl sites detected in each of the KEGG pathways, obtaining the acetylation coverage for each pathway: the ratio of acetylated sites to possible acetylation sites. To obtain a measure of the effect of SIRT3 in each pathway, the absolute value of the log2 fold change for each acetyl site in each pathway

was summed and divided by the number of sites, again on a per tissue basis. We calculated the standard score (z-score) of both the coverage and the summed magnitude fold change. A general outline of our code is found in accompanying text file (QSSA.txt). The overall pathway score was then calculated as the average of the individual z-scores:

$$\left(Z\left(\frac{n_s}{n_K}\right) + Z\left(\frac{1}{n_s}\sum_{s\,\in p}|FC_s|\right)\right)$$

The method was validated by comparing the results of QSSA with the results of over-representation biological pathway analysis.

Over-representation biological pathway analysis

KEGG pathway enrichment analysis was performed using the functional annotation tool of the DAVID bioinformatics resource (Huang et al., 2009a, b). Redundant proteins were removed from the data set and searched against a background that included all mouse proteins. Processes were sorted by Benjamini p-value with a significance cut off at $p < 0.05$. Only pathways containing five or more proteins were included in the analysis.

Western blotting

Antibodies for immunoblotting included anti-rabbit SIRT3 antibody (Cell Signaling Technology D22A3), anti-mouse VDAC1 as a mitochondrial loading control, pan-anti acetyl lysine (Cell Signaling Technology), and anti-His-HRP antibody (Abcam). The monoclonal antibody VDAC1 (clone N152B/23) was developed by and/or obtained from

the UC Davis/NIH NeuroMab Facility. Whole tissue lysates were boiled with SDS loading buffer and subjected to western blotting.

OXCT purification and activity assay

For site-specific acetyl-lysine incorporation, an acetyl-lysyl-tRNA synthetase/$tRNA_{CUA}$ pair that recognizes an amber codon was co-expressed with OXCT or TFAM (Neumann et al., 2009). The plasmid encoding human TFAM or human OXCT, pCDF pylT ($tRNA_{CUA}$), and pBK AcKRS (acetyllysine tRNA synthase) were co-transformed into electrocompetent CobB *E. coli* BL21DE3 cells. Overnight cultures were sub-cultured 1:100 into 2L of 2XYT containing spectinomycin (50 mg/ml), kanamycin (50 mg/ml), and ampicillin (150 mg/ml). Cultures were grown at 37°C with shaking to an OD_{600} of 0.6. Cells were supplemented with 10 mM N-ε-acetyllysine (Sigma-Aldrich) for 30 minutes and subsequently induced with 0.4 mM IPTG. Cells were grown overnight at 18°C, harvested by centrifugation, and purified by nickel chelating chromatography. SIRT3 was purified as previously described using nickel chelating chromatography (Hallows et al., 2006). Purified WT and acetylated OXCT was incubated with 0.5 mM NAD^+ and 1 mM DTT, with or without 2 μM SIRT3, in 50 mM Tris buffer (pH=7.6) at 4°C, overnight. As a negative control for background adjustment, purified acetylated TFAM was treated with SIRT3 in an identical manner. The activities of these enzymes were measured in 50 mM Tris buffer (pH =8.6) with 15 mM $MgCl_2$, using various concentration of succinyl-coA (Sigma), with 5mM acetoacetate (Sigma). Acetoacetyl-coA production was measured by absorbance at 310 nm using a plate reader. Kinetic parameters were fit to the Michaelis–Menten equation by least square fitting (MATLAB). For limited proteolytic

digestion 8 μM OXCT and 8 μM TFAM were treated with trypsin (1:100) for 4 hours in 50 mM Tris pH 7.5, 0.2 mM DTT. Peptides were separated from trypsin with a 10kDa spin filter. Peptides were incubated with 2 μM SIRT3 and 100 μM NAD^+ at 37°C for 0 or 4 hours. LC-MS detection of *O*AADPr was performed as described for metabolite analysis.

Ketone body utilization activity assay in brain homogenate

Brain cortices isolated from 8-month old, 24 hour fasted WT and *Sirt3*$^{-/-}$ mice (n=4) were placed in ice cold PBS supplemented with deacetylase inhibitors (1 mM sodium butyrate, 1 μM trichostatin A) and homogenized 3x1000 rpm with a glass homogenizer and Teflon pestle. The sample was centrifuged twice at 1000xg for 10 minutes at 4°C to remove insoluble material. The supernatant was used for the activity assay and protein was concentration was determined by BCA. To test acetoacetate utilization activity, homogenates were combined with 1 mM acetoacetate, 0.5 or 1 mM succinyl CoA, and 0.5 mM CoA in PBS at 37°C. A control reaction was performed without acetoacetate. Reaction time points were taken at 1, 3, 5, 8, 10, 12, 15, and 20 minutes by immediately quenching the reaction mixture in 9 volumes of ice cold methanol. Citrate synthase activity was monitored by combining homogenates with 0.5 mM oxaloacetate and 0.5 mM acetyl-CoA in PBS at 37°C. A control reaction was performed without oxaloacetate. Reaction time points were taken at 1 and 10 minutes by immediately quenching the reaction mixture in 9 volumes of ice cold methanol. All samples were centrifuged at 21000xg for 10 minutes and supernatants were diluted and further analyzed by reverse phase separation on a Synergy Hydro-RP column (100 mm x 2 mm, 2.5 μm particle

size, Phenomenex, Torrence, CA) coupled by negative mode electrospray ionization to an Orbitrap mass spectrometer, as previously described (Lu et al., 2010).

Sample preparation for metabolite analysis in brain

Brain cortices isolated from 15-month, 24 hour fasted WT and *Sirt3*$^{-/-}$ mice (n=4) were placed in 0.8 mL cold (-20°C) 80:20 methanol:H_2O (*v/v*) and homogenized 3x1000rpm with a glass homogenizer and Teflon pestle. The sample was centrifuged at 14000xg for 10 minutes at 4°C. The supernatant was transferred to a new tube on ice. The pellet was re-extracted with 0.5 mL cold (-20°C) 80:20 methanol:H_2O (*v/v*) twice, and the supernatants were combined. The samples were dried under nitrogen and resuspended in H_2O for LC-MS analysis as previously described (Lu et al., 2010). The results were normalized to tissue weight.

Supplemental References

Geer, L.Y., Markey, S.P., Kowalak, J.A., Wagner, L., Xu, M., Maynard, D.M., Yang, X., Shi, W., and Bryant, S.H. (2004). Open mass spectrometry search algorithm. J Proteome Res *3*, 958-964.

Hallows, W.C., Lee, S., and Denu, J.M. (2006). Sirtuins deacetylate and activate mammalian acetyl-CoA synthetases. Proceedings of the National Academy of Sciences of the United States of America *103*, 10230-10235.

Hastie, T., Tibshirani, R., and Friedman, J.H. (2009). The elements of statistical learning : data mining, inference, and prediction, 2nd edn (New York, NY: Springer).

Huang, D.W., Sherman, B.T., and Lempicki, R.A. (2009a). Bioinformatics enrichment tools: paths toward the comprehensive functional analysis of large gene lists. Nucleic Acids Res *37*, 1-13.

Huang, D.W., Sherman, B.T., and Lempicki, R.A. (2009b). Systematic and integrative analysis of large gene lists using DAVID bioinformatics resources. Nat Protoc *4*, 44-57.

Lu, W., Clasquin, M.F., Melamud, E., Amador-Noguez, D., Caudy, A.A., and Rabinowitz, J.D. (2010). Metabolomic analysis via reversed-phase ion-pairing liquid chromatography coupled to a stand alone orbitrap mass spectrometer. Anal Chem *82*, 3212-3221.

Neumann, H., Hancock, S.M., Buning, R., Routh, A., Chapman, L., Somers, J., Owen-Hughes, T., van Noort, J., Rhodes, D., and Chin, J.W. (2009). A method for genetically

installing site-specific acetylation in recombinant histones defines the effects of H3 K56 acetylation. Molecular cell *36*, 153-163.

Nguyen, N., Caruana, R (2007). Consensus Clusterings. Seventh IEEE International Conference on Data Mining (ICDM '07).

Wenger, C.D., Phanstiel, D.H., Lee, M.V., Bailey, D.J., and Coon, J.J. (2011). COMPASS: a suite of pre- and post-search proteomics software tools for OMSSA. Proteomics *11*, 1064-1074.